Phonon density of states probed by inelastic x-ray scattering

Alexey Bosak and Michael Krisch
European Synchrotron Radiation Facility, Boîte Postale 220, F-38043 Grenoble Cedex, France
(Received 6 September 2005; revised manuscript received 28 October 2005; published 22 December 2005)

The formalism and the experimental conditions under which coherent inelastic x-ray scattering from phonons can be utilized to determine the vibrational density of states are presented. The validity of the approach is checked by comparison of results for diamond and MgO with *ab initio* lattice dynamics calculations and thermodynamic measurements. For diamond the agreement between experiment and theory is remarkable, while for MgO slight differences can be observed, indicating the need for further refinement of the lattice dynamics calculations. The generalization of the formalism is discussed, and potential applications in various research fields are laid out.

DOI: 10.1103/PhysRevB.72.224305 PACS number(s): 63.20.Dj, 61.10.Eq, 78.70.Ck

I. INTRODUCTION

The experimental determination of the energy distribution function $g(E)$, or vibrational density-of-states (VDOS), gives important insight into the physical properties of materials, since it allows the derivation of many thermodynamic and elastic properties such as, for example, the specific heat, the vibrational entropy, the Debye temperature, and velocity.[1] If single crystals are available, the VDOS can in principle be derived from a Born-von Kármán (BvK) fit to the experimentally determined phonon dispersion curves. Usually these dispersions are, however, recorded only along the main crystallographic directions. For nontrivial directions the convergence to the real dispersion is not guaranteed, and consequently the thus-obtained VDOS is only approximate. The proper procedure necessitates a uniform sampling inside the irreducible part of the first Brillouin zone (BZ) with a subsequent interpolation, which is not subjected to the influence of a model.[2] This approach is much more time consuming and therefore rarely used.

In cases where sufficiently perfect single crystals are not available, or for noncrystalline systems such as liquids and glasses, $g(E)$ has to be determined directly. This is commonly done by inelastic neutron scattering (INS). For incoherent monoatomic scatterers, the inelastic scattering spectra are, after proper correction for the Debye-Waller factor and multiphonon contributions, directly proportional to $g(E)$. For coherent scatterers the reconstruction of the VDOS from the INS spectra necessitates (*i*) a correct directional averaging in polycrystalline samples and (*ii*) an appropriate reciprocal space sampling.[3–5] The sampling procedure of this so-called "incoherent approximation" is usually obtained empirically. For systems with different atomic species, only the generalized density of states can be obtained, for which the individual contributions of the different constituent atoms are weighted by their corresponding scattering length.

For elements with a Mössbauer isotope, the VDOS can be obtained by nuclear inelastic scattering (NIS).[6,7] In this method, the nuclear resonance fluorescence, following the absorption of x rays from Mössbauer nuclei, is recorded. This process occurs on the time scale of the lifetime of the nuclear resonance. Exploiting the time structure of synchrotron radiation and using timing electronics allows the selective detection of only the resonantly excited quanta. Tuning the energy of a highly monochromatized synchrotron beam through the Mössbauer resonance while monitoring the fluorescence yield then provides a direct measure of the VDOS. The technique is limited to elements possessing a Mössbauer isotope. This can, on the other hand, turn into an important advantage for multi-element materials, since the dynamics of the resonant nuclei can be studied separately.

As inelastic x-ray scattering (IXS) from phonons is essentially a coherent scattering process, the same incoherent approximation as for coherent INS can be applied. Here, we present a detailed description of the theoretical background applied to IXS and show results on a monoatomic and binary system, namely diamond and MgO. These results are confronted with available *ab initio* lattice dynamics calculations, and our derived elastic and thermodynamic properties are compared to values available in literature. The applicability and the limitations of this novel spectroscopic technique, as well as potential applications, are discussed in the conclusions.

II. THEORETICAL BACKGROUND

A. General formalism

The dynamical structure factor for IXS within the limit of one-phonon scattering can be written as[8]

$$S(\vec{Q},E,T) = \sum_j G(\vec{Q},j)F(E,T,\vec{Q},j), \tag{1}$$

where $G(\vec{Q},j)$ is

$$G(\vec{Q},j) = \left| \sum_n f_n(\vec{Q}) e^{i\vec{Q}\vec{r}_n - W_n} (\vec{Q}\cdot\hat{\sigma}_n(\vec{Q},j)) M_n^{-1/2} \right|^2 \tag{2}$$

and the thermal factor is given by

$$F(E,T,\vec{Q},j) = \frac{\left\{\left[\exp\left(\frac{E_{\vec{Q},j}}{kT}\right)-1\right]^{-1}+\frac{1}{2}\pm\frac{1}{2}\right\}}{E_{\vec{Q},j}}\cdot\delta(E\mp E_{\vec{Q},j}). \tag{3}$$

Here $\vec{Q}$ denotes the momentum transfer, E is the frequency of the phonon, T is the temperature, and k_B is the Boltzmann constant. The sum in Eq. (2) extends over atoms in the unit cell. $f_n(\vec{Q})=f_n(|\vec{Q}|)\equiv f_n(Q)$ is the atomic form factor of atom n at position $\vec{r}_n$, $\hat{\sigma}_n(\vec{Q},j)$ is its eigenvector component in mode j, M_n is its mass, and W_n is the corresponding Debye-Waller factor. The upper and the lower signs in Eq. (3) correspond to phonon creation and annihilation, respectively. An alternative definition of the polarization vectors is $\hat{\sigma}_n(\vec{Q},j)=\exp(i\vec{Q}\cdot\vec{r}_n)\cdot\hat{e}_n(\vec{Q},j)$, and the transformation rules are $\hat{e}_n(\vec{Q},j)=\exp(-i\vec{\tau}\cdot\vec{r}_n)\cdot\hat{e}_n(\vec{Q}-\vec{\tau},j)$, where $\vec{\tau}$ is an arbitrary reciprocal lattice vector. If the Debye-Waller factors are assumed to be the same for all types of atoms ($\tilde{W}$), we obtain for the averaging over the sphere of radius $Q=|\vec{Q}|$

$$S(Q,E,T) = g(Q,E)F(E)\cdot\exp(-2\tilde{W}), \tag{4}$$

$$g(Q,E) = \left\langle\left|\sum_n f_n(Q)(\vec{Q}\cdot\hat{e}_n(\vec{Q},j))M_n^{-1/2}\right|^2\delta(E-E_{\vec{Q},j})\right\rangle, \tag{5}$$

where $\langle\cdots\rangle$ means averaging over the sphere of radius Q and the phonon modes j; the thermal factor is given by

$$F(E) = [\exp(E/kT)-1]^{-1}E^{-1}. \tag{6}$$

For large Q the normalized $g(Q,E)$ should approach the generalized DOS:

$$g(Q,E)\to AQ^2\cdot\sum_n\frac{G_n(E)}{M_n}\cdot f_n^2(Q), \tag{7}$$

where $G_n(E)=\Sigma_{\vec{Q},j}|\hat{e}_n(\vec{Q},j)|^2\delta(E-E_{\vec{Q},j})$ are the partial densities of states and A is a scaling factor. For moderate values of Q the function $g(Q,E)$ has to be calculated directly from the lattice dynamic model.

B. Sampling optimization

Several aspects have to be considered in order to ensure a correct VDOS approximation. Intuitively, the larger the momentum transfer, the better the approximation, and in the limit of a very large Q sphere, even one IXS spectrum will give a good VDOS approximation. However, the radius of the largest Q sphere is given by the maximum scattering angle of the IXS spectrometer. Typical values and the corresponding energy resolution for the ID28 spectrometer at the ESRF are indicated in Table I. The momentum transfer range corresponding to the first Brillouin zone has to be excluded, since in this case the total momentum transfer $\vec{Q}$ is equal to the phonon wave vector $\vec{q}$, and only phonon modes with an eigenvector component parallel to $\vec{q}$ acquire finite intensity [see Eq. (2)]. Another aspect concerns the thickness of the integration shell. While for INS there are no constraints associated to this, since the neutron scattering length b is independent of Q, for IXS the atomic form factor $f(Q)$ displays a pronounced Q dependence with an approximately exponential decay, cast into the following form:[9] $f(Q)=\Sigma_{i=0}^{3}a_i\exp(-b_iQ^2)+c$. This decay is element dependent, and the half-value of $f(Q)$ corresponds roughly to the inverse of the spatial extent of the atom. This leads to a distortion of the VDOS, if the integration is performed over a large Q range.

TABLE I. Spectrometer characteristics for selected x-ray energies.

Reflection	Energy (eV)	Wavelength (Å)	Resolution (meV)	Q_{max} (nm^{-1})
(8 8 8)	15816	0.7839	5.4	~70
(9 9 9)	17793	0.6968	3.0	~80
(11 11 11)	21748	0.5701	1.8	~95

In general, no recipe exists for the choice of the shell sampling, but in some special cases one can make semiquantitative estimations for preferable settings. If the averaging is performed over a specific Q range with $Q_{min}<Q<Q_{max}$, indicated by the second parenthesis, we obtain from Eq. (5):

$$g(Q_{min},Q_{max},E) = \left\langle\left\langle\sum_n\frac{f_n^2}{M_n}|\vec{Q}\cdot\hat{e}_n(\vec{Q},j)|^2\delta(E-E_{\vec{Q},j})+\sum_{n\neq m}\frac{f_nf_m}{\sqrt{M_nM_m}}\times(\vec{Q}\cdot\hat{e}_n(\vec{Q},j)\ \cdot(\vec{Q}\cdot\hat{e}_m^*(\hat{Q},j)\ \delta(E-E_{\vec{Q},j})\right\rangle\right\rangle. \tag{8}$$

As the desired approximation is

$$g(Q_{min},Q_{max},E)\to A\cdot\langle Q\rangle^2\cdot\sum_n\frac{f_n(\langle Q\rangle)^2}{M_n}G_n(E), \tag{9}$$

the two following conditions have to be approximately satisfied, corresponding to a uniform sampling of the BZ [Eq. (10a)] and to the uniform mutual annihilation of cross terms over the BZ [Eq. (10b)]:

$$\left\langle\left\langle\sum_n\frac{f_n^2}{M_n}|\vec{Q}\cdot\hat{e}_n(\vec{Q},j)|^2\delta(E-E_{\vec{Q},j})\right\rangle\right\rangle \to A\langle Q\rangle^2\cdot\sum_n\frac{f_n(\langle Q\rangle)^2}{M_n}G_n(E), \tag{10a}$$

$$\left\langle\left\langle\sum_{n\neq m}\frac{f_nf_m}{\sqrt{M_nM_m}}(\vec{Q}\cdot\hat{e}_n(\vec{Q},j)\ \cdot(\vec{Q}\cdot\hat{e}_m^*(\vec{Q},j)\ \delta(E-E_{\vec{Q},j})\right\rangle\right\rangle\to 0. \tag{10b}$$

No analytic solution is available for such a problem, and the calculations have to be performed numerically.

1. Uniformity of sampling

The uniformity of sampling was checked by a direct numerical calculation: for every mesh point (N points inside the BZ, mesh step: $0.025a^*$) within the BZ its weight is taken equal to the number of translationally equivalent points within the sampling shell. As a measure of uniformity of sampling the standard deviation of the weight of points w from its average $\bar{w}$ over the BZ is taken:

$$U_r = \left(1/N \sum_{BZ} (w - \bar{w})^2 \right)^{1/2}. \tag{11}$$

The smaller U_r is, the better is the uniformity of sampling.

2. Uniformity of annihilation of cross terms

To estimate the uniformity of annihilation of cross terms, the weight of every mesh point is taken equal to the sum over translationally equivalent points within the sampling shell with ±1 weight, and the standard deviation of the weight of points from zero over the BZ is then calculated:

$$C_r = \left(1/N \sum_{BZ} w^2 \right)^{1/2}. \tag{12}$$

For the uniformity of sampling the output function depends on the BZ shape only, whereas the uniformity of annihilation of cross terms depends also on the cell content. Once the parameters are established, the quality of sampling for an arbitrary composition (within a given type of structure) can be easily estimated by defining a parameter of merit:

$$M_r = \left[\sum_n \left(\frac{\bar{f}_n^2}{M_n} \right)^2 \cdot U_r^2 + \sum_{n \neq m} \left(\frac{\bar{f}_n \bar{f}_m}{\sqrt{M_n M_m}} \right)^2 \cdot C_r(n,m)^2 \right]^{1/2} \times \left(\sum_n \bar{f}_n \right)^{-2}, \tag{13}$$

where $\bar{f}_n$ corresponds to the average value of the form factor over the sampled shell thickness.

For example, for diamond-type structures the atoms of the basis are located at the origin and at 1/4 along the cube diagonal [C1 (0 0 0) and C2(1/4 1/4 1/4)]:

$$(\vec{Q} \cdot \hat{e}_{C1}(\vec{Q},j)) = (\vec{Q} \cdot \hat{e}_{C1}(\vec{q},j)),$$

$$(\vec{Q} \cdot \hat{e}_{C2}(\vec{Q},j)) = (\vec{Q} \cdot e_{C2}(\vec{q},j) \cdot \exp\left(\frac{\pi i}{2}(h+k+l) \right),$$

$$(\vec{Q} \cdot \hat{e}_{C1}(\vec{Q},j) \cdot (\vec{Q} \cdot \hat{e}^*_{C2}(\vec{Q},j)) = \begin{cases} (\vec{Q} \cdot \hat{e}_{C1}(\vec{q},j) \cdot (\vec{Q} \cdot \hat{e}^*_{C2}(\vec{q},j)), & h+k+l = 4n, \\ -(\vec{Q} \cdot \hat{e}_{C1}(\vec{q},j) \cdot (\vec{Q} \cdot \hat{e}^*_{C2}(\vec{q},j)), & h+k+l = 4n+2, \\ -i(\vec{Q} \cdot \hat{e}_{C1}(\vec{q},j) \cdot (\vec{Q} \cdot \hat{e}^*_{C2}(\vec{q},j)), & h+k+l = 4n+1, \\ i(\vec{Q} \cdot \hat{e}_{C1}(\vec{q},j) \cdot (\vec{Q} \cdot \hat{e}^*_{C2}(\vec{q},j)), & h+k+l = 4n+3. \end{cases}$$

Here, we introduce the reduced phonon wave vector $\vec{q}$ defined inside the first Brillouin zone, which is connected to the total momentum transfer $\vec{Q}$ via the reciprocal lattice vector $\vec{\tau}$ ($\vec{Q} = \vec{\tau} + \vec{q}$). Terms $(\vec{Q} \cdot \hat{e}_{C1}(\vec{Q},j) \cdot (\vec{Q} \cdot \hat{e}^*_{C2}(\vec{Q},j))$ mutually annihilate in pairs corresponding to zones with $h+k+l=4n(w=+1)/h+k+l=4n+2(w=-1)$ and $h+k+l=4n+1(w=+1)/h+k+l=4n+3(w=-1)$. We therefore obtain two parameters, $C_r(1)$ and $C_r(2)$, for the uniformity of annihilation of cross terms, and the parameter of merit takes the following form:

$$M = \sqrt{U_r^2 + C_r(1)^2 + C_r(2)^2}. \tag{14}$$

This value is displayed in a three-dimensional plot in Fig. 1(a) as a function of Q_{min} and the shell thickness $Q_{max} - Q_{min}$ in units of the inverse lattice parameter. It is important to note that the above procedure corresponds to the worst scenario, in particular, we neglect the annihilation of cross terms due to both accidental and regular degeneracy (crossing of two phonon branches and degenerate transverse phonon branches, respectively). The annihilation we are dealing with is only due to the phase shift in different Brillouin zones, and the actual situation is always closer to a perfect averaging.

For NaCl-type structures the atoms of the unit cell are located at the origin and at 1/2 along the cube diagonal [Na (0 0 0) and Cl (1/2 1/2 1/2)]:

$$(\vec{Q} \cdot \hat{e}_{Na}(\vec{Q},j)) = (\vec{Q} \cdot \hat{e}_{Na}(\vec{q},j)),$$

$$(\vec{Q} \cdot \hat{e}_{Cl}(\vec{Q},j)) = (\vec{Q} \cdot \hat{e}_{Cl}(\vec{q},j) \cdot \exp(\pi i(h+k+l)),$$

$$(\vec{Q} \cdot \hat{e}_{Na}(\vec{Q},j)) \cdot (\vec{Q} \cdot \hat{e}^*_{Cl}(\vec{Q},j)) = \begin{cases} (\vec{Q} \cdot \hat{e}_{Na}(\vec{q},j) \cdot (\vec{Q} \cdot \hat{e}_{Cl}(\vec{q},j), & h+k+l = 2n, \\ -(\vec{Q} \cdot \hat{e}_{Na}(\vec{q},j) \cdot (\vec{Q} \cdot \hat{e}_{Cl}(\vec{q},j), & h+k+l = 2n+1. \end{cases}$$

The U_r [Eq. (11)] parameter is obviously the same as for diamond. The parameter of merit for MgO is given in Fig. 1(b).

It is important to note that the developed criteria above are independent of any specific lattice dynamics model, but result from simple symmetry considerations. The advantage of its use is that no *a priori* knowledge of the lattice properties is needed.

In order to extract the VDOS from the experimental spectra, the contribution from multi-phonon processes and the resolution function have to be properly subtracted. The involved procedures are discussed in the following chapter.

C. X-VDOS reconstruction

1. Inelastic scattering probability and vibrational density of states

Assuming a quasi-harmonic lattice with well-defined phonon states, the probability of inelastic scattering $W(E)$ can be expanded in terms of n-phonon contributions[10]

$$W(E) = f_{LM} \left(\delta(E) + \sum_{n=1}^{\infty} S^{(n)}(E) \right), \tag{15}$$

where f_{LM} is the Lamb-Mössbauer factor (probability of recoilless scattering). The VDOS $g(E)$ is directly proportional to the single-phonon term in the expansion:

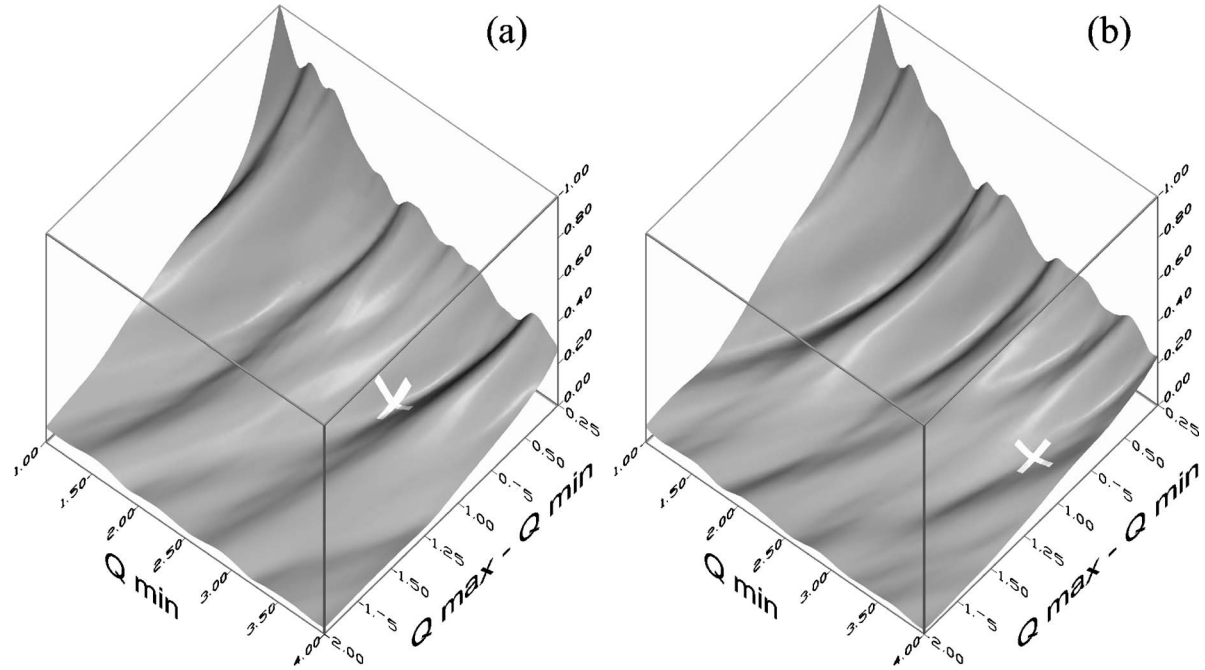

FIG. 1. Estimated sampling quality for two selected structures: (a) diamond and (b) MgO. Q is given in units of the inverse lattice parameter. The favorable points used in this study are marked by crosses.

$$S^{(1)}(E) = \int \frac{d\tau}{2\pi} \exp(-iE\tau) M(\tau) = \frac{E_R g(|E|)}{E[1-\exp(-E/k_B T)]}. \tag{16}$$

Here, $E_R = \hbar^2 k^2 / 2M$ is the recoil energy of a free nucleus of mass M, and $M(\tau)$ is the time-dependent correlation function, which describes the correlation between the displacement $\boldsymbol{u}$ of the nucleus at a time interval $t = \hbar\tau$.[10] The multiphonon contributions can be obtained recursively as

$$S^{(n)}(E) = \frac{1}{n} S^{(1)}(E) \otimes S^{(n-1)}(E). \tag{17}$$

In the following, the data treatment from the raw experimental spectra to the properly normalized VOS shall be presented. Since the procedures closely follow the ones as previously described in great detail,[11] we outline here only the main steps.

2. Deconvolution procedure and subtraction of multi-phonon contributions

The first step consists of the careful subtraction of the elastic contribution from the experimental data. The thus-corrected inelastic energy spectrum $I(E)$, which only contains the inelastic part, can be normalized according to Lipkin's sum rules[12]

$$\int I(E) dE = I_0 (1 - f_{LM}), \tag{18a}$$

$$\int I(E) E dE = I_0 E_R, \tag{18b}$$

where I_0 is a scaling factor. In their present form Eq. (18b) is valid for a symmetric, normalized instrumental resolution function $P(E)$ [$\int P(E) dE = 1$ and $\int P(E) E dE = 0$]. Equations (18a) and (18b) thus allow the determination of I_0 and f_{LM}.

In the further treatment, the multi-phonon term is eliminated simultaneously with the deconvolution of the instrumental function. To this purpose $Q(\tau)$ and $M(\tau)$, the Fourier transform of the instrumental resolution function $P(E)$ and the inelastic energy spectrum $I(E)$, respectively, are introduced:

$$Q(\tau) = \int dE \exp(iE\tau) P(E), \tag{19a}$$

$$J_0(\tau) = \int dE \exp(iE\tau) I(E). \tag{19b}$$

Furthermore, using $Q_0(\tau) = (Q(\tau) + P_{if})/(1 + P_{if})$, where P_{if} is a numerical parameter defining the degree of deconvolution, one obtains for the Fourier transform of the single-phonon scattering term $S_1(E)$

$$M(\tau) = \ln\left(1 + \frac{\int dE \exp(iE\tau) I(E)}{I_0 f_{LM} Q_0(\tau)}\right) \tag{20}$$

and, via back-transformation the frequency distribution function,

$$g(E) = \frac{E}{E_R}[1 - \exp(-E/kT)] \int \frac{d\tau}{2\pi} \exp(-iE\tau) M(\tau). \tag{21}$$

3. Renormalization of the low-energy part of X-VDOS

As was already mentioned above, in the case of non-monoatomic crystals only a generalized VDOS can be obtained. It can, however, be shown that the real VDOS can be recovered at least for the low-energy part. The generalized X-VDOS $\tilde{g}(E)$, normalized to unity $[\int_E \tilde{g}(E)dE = 1]$, for a crystal containing N (different) atoms is given by

$$\tilde{g}(E) = N \sum_n \frac{G_n(E)}{M_n} \cdot \bar{f}_n^2 \Bigg/ \sum_n \frac{\bar{f}_n^2}{M_n}. \tag{22}$$

If we keep in mind that the low-energy range of the X-DOS corresponds to phonons of comparably large wavelengths, the displacement of different atom species can be considered approximately equal: $|\hat{e}_n|^2/M_n = |\hat{e}_m|^2/M_m$.

As $g(E) = \Sigma_n G_n(E)$, the generalized DOS at low energies can be written as

$$\tilde{g}(E) = g(E) \sum_n \bar{f}_n^2 \Bigg/ \sum_n M_n. \tag{23}$$

In this manner, the properly normalized low-energy limit of the real VDOS can be found:

$$g(E) = \tilde{g}(E) \cdot \frac{1}{N} \sum_n \frac{\bar{f}_n^2}{M_n} \cdot \sum_n M_n \Bigg/ \sum_n \bar{f}_n^2 = \tilde{g}(E) \cdot \alpha. \tag{24}$$

This allows, even in multi-component systems, the determination of material properties such as the low-temperature limit of θ_D and the effective sound speed.

III. EXPERIMENTAL DETAILS

The experiment was performed on the Inelastic Scattering beamline ID28 at the European Synchrotron Radiation Facility. The instrument was operated utilizing the silicon (8 8 8) and (9 9 9) setup, providing a total energy resolution of 5.4 and 3.0 meV, respectively. The highly monochromatized x rays were focused by a toroidal mirror into a spot size of 250×100 μm^2 (horizontal $\times$ vertical, full-width-half-maximum). The momentum transfer was selected by rotating the analyzer arm around the sample position in the horizontal plane. The spectrometer arm is equipped with five analyzers, and therefore five spectra are recorded simultaneously. The momentum resolution was set to 0.7 nm^{-1} both in horizontal and vertical directions. The spectra were recorded for two angular settings of the spectrometer arm, thus covering a Q range of about 15 nm^{-1} and yielding ten IXS spectra. The exact angular positions were chosen to have an appropriate sampling for the X-VDOS reconstruction (see above) and to avoid Bragg peaks.

The resolution functions were experimentally determined from a PMMA sample, kept at 10 K, and at $Q = 10$ nm^{-1}. The thus-obtained resolution functions are almost identical. For the deconvolution procedure the individual resolution functions were replaced by the best fit of a pseudo-Voigt function to the average of the five experimental resolution functions. The relative efficiencies of the analyzers were determined using the elastic scattering from a PMMA sample at the same angular position of the spectrometer as the ones used for the VDOS measurements. These were then subsequently used in order to properly weight the contribution of the individual analyzers in the summation of the IXS spectra. The spectra were recorded for the energy loss side (Stokes), including the elastic line, centered around zero energy transfer. The energy gain side (anti-Stokes) was constructed from the detailed balance condition, prior to the deconvolution procedure.

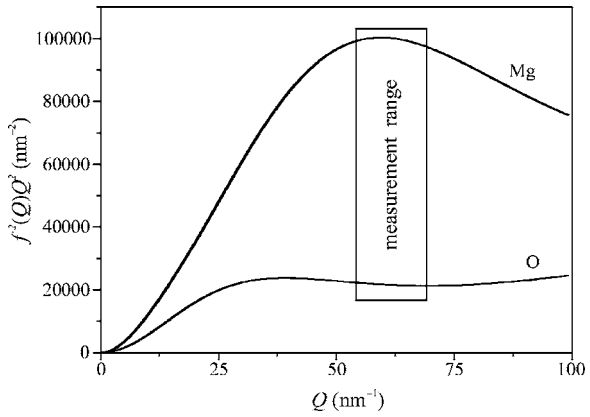

FIG. 2. Effective scattering factors $f^2(Q)Q^2$ for Mg and O.

Single-crystal diamond powder with an average grain size of 3–5 μm and MgO powder, obtained by grinding a single crystal, was used. The compacted powders were placed in aluminum holders between 8 μm thick Kapton® foils (3 mm thick/$\varnothing$3 mm for diamond and 1.5 mm thick/$\varnothing$2 mm for MgO). In the case of MgO, the sample thickness corresponds closely to the optimum thickness $t_{\text{opt}} = 1/\mu$, where μ is the photoelectric absorption thickness. For diamond the effective sample length is limited to 3 mm due to the depth of field of the spectrometer. The resulting effective scattering volumes thus amount to 0.08 and 0.04 mm^3 for diamond and MgO, respectively.

In the case of diamond the VDOS can be directly obtained, if the experimental spectra are properly weighted by the factor $f(Q)^{-2}Q^{-2}$ [see Eq. (5)]. For MgO we can only extract the X-VDOS for the selected Q region. The weighting with $f(Q)^{-2}$ Q^{-2} is no more useful as the contributions for the two atoms are significantly different. On the other hand, the variation of effective scattering factors $f(Q)^2$ Q^2 for Mg and O is less than 8% over the sampled Q range (see Fig. 2), therefore no correction is needed.

IV. RESULTS AND DISCUSSION

A. Diamond

The measurements for diamond were performed with both 5.4 and 3.0 meV energy resolution. For the higher energy resolution the spacing between integration points was

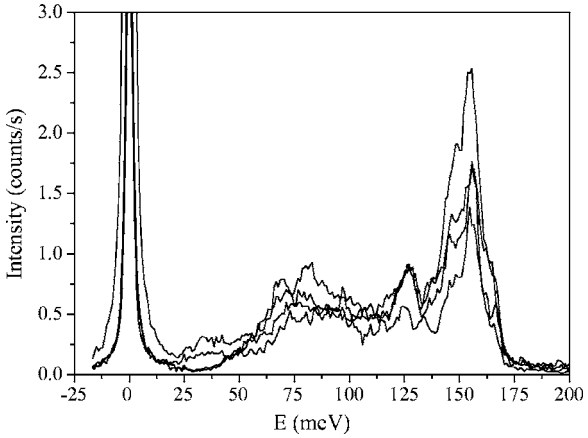

FIG. 3. Raw IXS spectra of polycrystalline diamond at scattering angles of 45.5°, 47.0°, 48.5°, and 50.0°. The instrumental energy resolution was 3.0 meV.

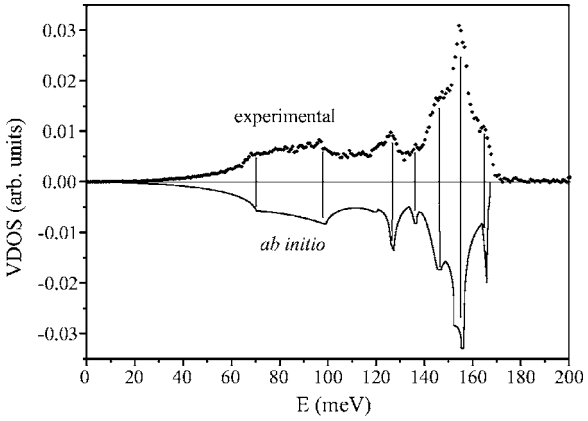

FIG. 5. Reconstructed vibrational density of states of diamond versus calculated *ab initio* results.[13] The data are normalized to equal surfaces.

0.9 meV, the total acquisition time for each point ~235 s (200 mA storage ring operation mode), and the maximal inelastic count rate ~2.5 s^{-1}; for the lower energy resolution the spacing between integration points was 1.8 meV, the total acquisition time for each point ~200 s (200 mA storage ring operation mode), and the maximal inelastic count rate ~10 s^{-1}. An example of the raw high-resolution spectra is shown in Fig. 3.

The results of the properly weighted and summed IXS spectra, recorded at the two incident photon energies, are shown in Fig. 4. We note that besides differences in the visibility of certain features (due to the different energy resolutions), the X-DOS spectra recorded at 15 816 and 17 794 eV are very similar, despite the fact that the exact Q positions of the analyzers are slightly shifted due to the difference in photon energy. This confirms to some extent the validity of the sampling procedure. Hereafter only the high-resolution data will be discussed.

The deconvolution procedure gives a physically reasonable value of the Lamb-Mössbauer factor of ~0.85 and a multiphonon contribution of about 8% of the total inelastic part. Our obtained single-phonon VDOS agrees well with the *ab initio* calculated one,[13] as can be appreciated in Fig. 5. The position of special points is nearly identical, and furthermore the high-energy peak, due to the overbending of the optical phonon branch,[13–15] is clearly seen.

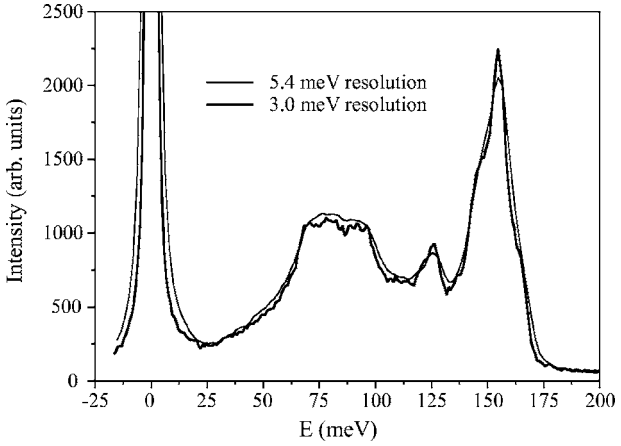

FIG. 4. "Incoherent" inelastic scattering spectra of polycrystalline diamond, recorded at 15 816 eV (5.4 meV energy resolution) and 17 794 eV (3.0 meV energy resolution). The intensity is approximately normalized to equal x-ray exposures.

The excellent quality of our experimental VDOS allows the determination of several macroscopic parameters. For example, the specific heat at constant volume is obtained by Eq. (25), if the VDOS is normalized to unity:[1]

$$C_v = 3Nk_B \int_0^{E_{\max}} \left(\frac{E}{k_B T}\right)^2 \frac{\exp(E/k_B T) g(E) dE}{[\exp(E/k_B T) - 1]^2}, \qquad (25)$$

whereas the Debye temperature θ_D is obtained formally from the Debye equation.[16] Their temperature evolution is displayed in Fig. 6. For C_V our results are in good agreement with other experimental data: within ~2% below 100 K (Ref. 17) and between 300 and 1100 K.[18] The largest discrepancy occurs at ~200 K and amounts to about 10%. The sudden drop of the Debye temperature below 70 K is an artifact due to the low signal level approaching zero energy transfer. Nevertheless, a parabolic fit to the low-energy part of the VDOS (from 0 to 25 meV) allows the determination of the average sound speed v_D. Our value for v_D is in excellent agreement with the average sound speed calculated from elastic constants[19] according to

$$v_D = \left(\frac{1}{12\pi} \sum_{j=1}^{3} \int \frac{1}{V_j^3} d\Omega\right)^{-1/3}, \qquad (26)$$

where v_j are found from the Christoffel's equation. The low-temperature limit of θ_D, obtained from the same fit to the VDOS, is obviously also very close to the calculated one:

$$\theta_D = \nu_D \frac{\hbar}{k_B} \left(\frac{6N_A \pi^2}{V_m}\right)^{1/3}. \qquad (27)$$

Table II summarizes the main results. Further quantities which can be derived are mean-squared thermal displacement $\langle (\Delta x)^2 \rangle = -\ln f_{\mathrm{LM}}/k^2 = 0.002$ Å^2 (k is the wave vector of the incident photon); mean kinetic energy $\langle T \rangle \sim 370$ K at

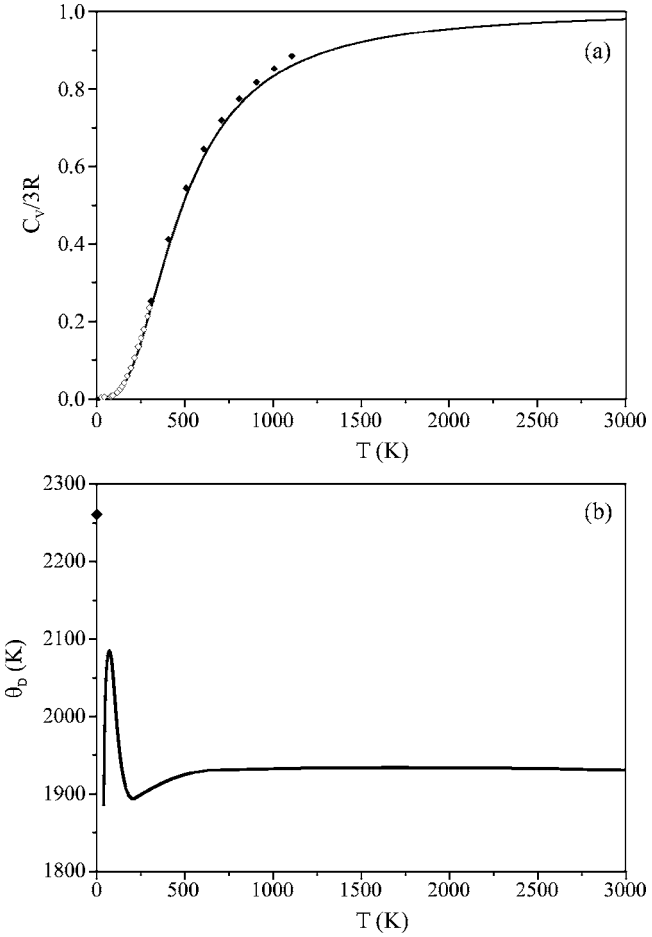

FIG. 6. (a) Specific heat C_V (solid line) and (b) Debye temperature θ_D (solid line) calculated from the experimental VDOS. Thermodynamic results for the low-T (open diamonds)[17] and high-T C_V data (full diamonds)[18] are shown as well. The solid diamond in panel (b) indicates the zero-temperature θ_D, derived from a parabolic fit to the VDOS.

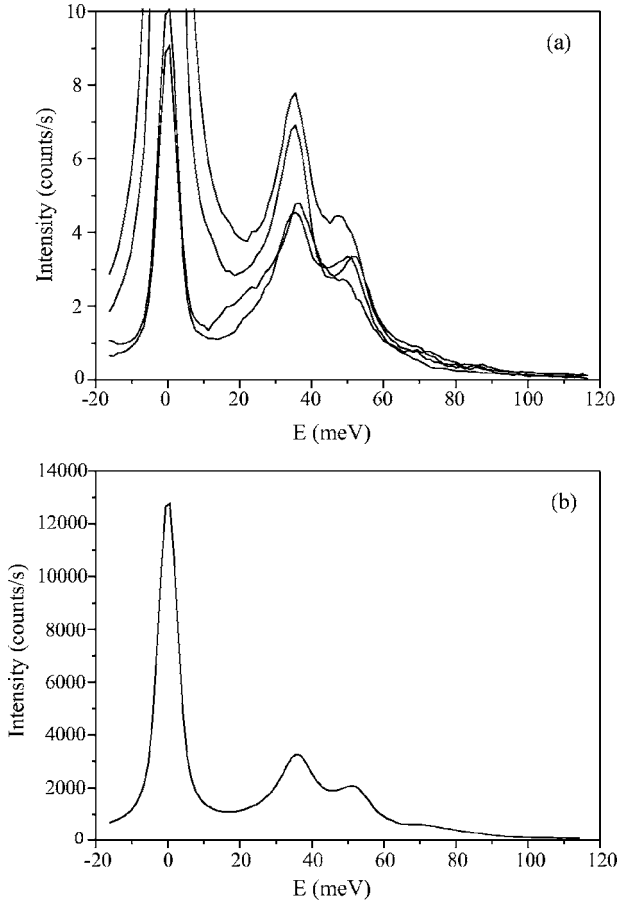

FIG. 7. (a) Raw IXS spectra of MgO powder at scattering angles of 45.3°, 46.8°, 48.3°, and 49.8° and (b) "incoherent" scattering spectrum.

room temperature; and mean force constant $\langle F \rangle \sim 775$ N/m.[20]

B. Magnesium oxide

The measurements on MgO were performed with 5.4 meV energy resolution. The spacing between integration points was 1.2 meV, the total acquisition time for each point ~500 s (90 mA storage ring operation mode), and the maximal inelastic count rate ~10 s^{-1}. An example of raw spectra is given in Fig. 7. The much stronger elastic contribution for two out of the four spectra is due the proximity of a Bragg peak.

TABLE II. Selected macroscopic parameters for diamond.

Parameter	Calculated from VDOS	Other experimental data
θ_D—high temperature	1930(40) K	1860 K (Ref. 21)
θ_D—low-temperature limit	2250(50) K	2240 K (Ref. 19)
average sound speed	13.55(30) km/s	13.46 km/s (Ref. 19)

The same procedure of deconvolution and multiphonon substraction as for diamond is formally applied to MgO. The recoil factor is used as fitting parameter, and its value, for which the multiphonon contribution is properly removed, is close to the Mg recoil factor (~5 meV). Figure 8 shows the comparison of the experimental X-VDOS with results from different *ab initio* calculations.[22–25] As expected, the overall form of the X-VDOS is roughly the same as for the VDOS, but relative intensities of peaks are changed due to the different scattering power of Mg and O for x rays. As none of the calculations match the experimentally determined phonon dispersion perfectly,[26,27] there are consequently significant differences in the VDOS as well. These concern the two main peaks, centered around 36 and 52 meV, and the high-energy cutoff. The best agreement between experiment and theory is obtained for calculations using density functional perturbation theory (DFPT) within the local density approximation (LDA).[22,23] The calculations by Drummond *et al.*,[24] performed using DFT within the quasi-harmonic approximation, underestimate the transverse acoustic (TA) phonon energies and overestimate the energies of the highest optical

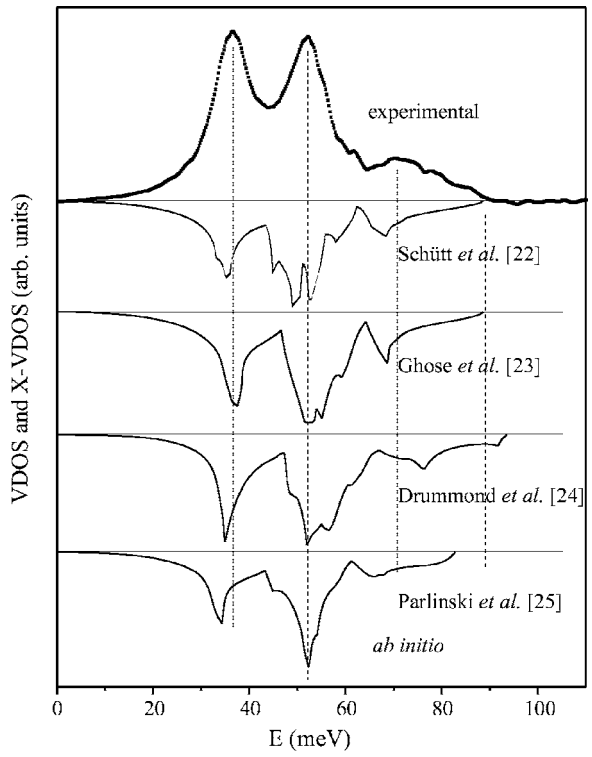

FIG. 8. Reconstructed generalized X-VDOS of MgO versus calculated *ab initio* results.

branches. The calculation by Parlinski *et al.*[25] shows the largest energy difference for the first peak in the VDOS (~4 meV) and significantly underestimates the energy of the highest optical branches.

As only the X-VDOS is available, no thermodynamic data can be obtained. The present data should be completed by N-VDOS measurements in order to obtain the partial VDOS for Mg and O, or, less directly, the present X-VDOS results should be used for the adjustment of *ab initio* models, most likely using DFPT within LDA. As discussed in Sec. II C 3, it can be shown that the real VDOS can be obtained at least for the low-energy part. For this portion of the VDOS ($E < 20$ meV) we obtain a scaling factor α of about 0.908 and extract from the thus-corrected generalized VDOS the low-temperature limit of the Debye temperature and the average sound speed by a parabolic fit to the experimental data. In Table III we compare our results with the ones calculated from available elastic data. The agreement is remarkable, thus proving that even for a multi-component system aggregate properties can be correctly extracted.

C. Applicability and limitations of the method

The general applicability of the method for the study of elementary solids can be easily estimated. The overall scattered intensity is proportional to $nsf^2(\langle Q \rangle) \cdot \exp(-s/\lambda)$, where n is the concentration of scatterers, s is the sample thickness, and λ is the x-ray attenuation length ($\lambda = 1/\mu$). The optimum signal is attained, if $s = \lambda$; on the other hand s must not exceed the focal depth of field of the Rowland-type spectrometer. For the ID28 spectrometer the depth of field is given by 2 mm/sin(θ_s), where 2 mm corresponds to the horizontal size of the detector pinhole and θ_s is the scattering angle. For typical VDOS setups the depth of field is limited to about 3 mm. As can be seen from Fig. 9(a), where we take a thickness cutoff equal to 3 mm, in the worst case the scattered intensity is only six times lower than in our experiment (equivalent diamond thickness for a powder is taken as 2 mm).

TABLE III. Selected macroscopic parameters for MgO.

Parameter	Calculated from VDOS	Calculated from elastic data[28]
θ_D—low-temperature limit	935(20) K	940 K
average sound speed V_D	6.63(13) km/s	6.65 km/s

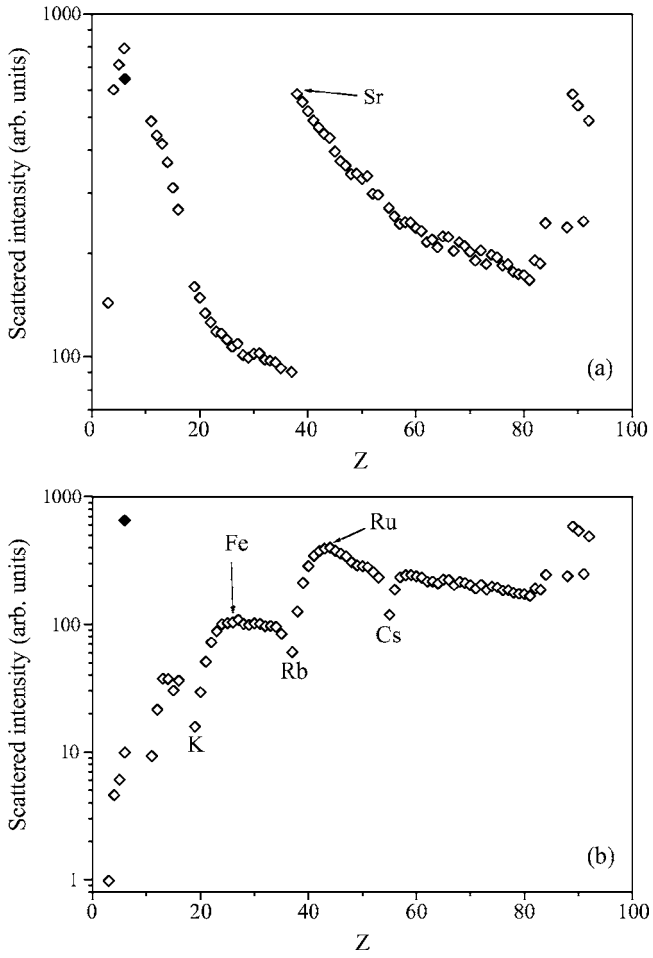

FIG. 9. Relative inelastic scattering intensity of elementary solids of mass number Z for an incident photon energy of 15.8 keV, $Q = 63$ nm^{-1}, and for an optimum sample thickness, but not thicker than 3 mm (a, upper panel) or a sample thickness of 20 μm (b, bottom panel).

As a consequence, the X-VDOS can be determined with an appropriate accuracy for essentially all elemental solids. One of the potential applications of this novel technique is the VDOS determination of samples submitted to high pressures. The most commonly used high-pressure device is the diamond anvil cell (DAC). Taking as a benchmark a typical thickness of 20 μm, the corresponding dependence of the scattering intensity as a function of Z is shown in Fig. 9(b). It

is obvious that for low Z materials, the mismatch of the acceptable sample thickness and the attenuation length λ is so large that the scattered intensity is very weak. For elements heavier than, say, scandium, however, the signal level should be sufficiently high to allow measurements in a DAC.

V. CONCLUSIONS

Inelastic x-ray scattering within the "incoherent approximation" approach promises to become a valuable tool in the determination of the frequency distribution function, thus complementing well-established inelastic neutron and nuclear scattering techniques. Our criteria developed for a uniform sampling allow the reliable determination of the VDOS, as demonstrated for the case of diamond, used as a benchmark. We obtain a very good agreement of our X-VDOS and derived elastic and thermodynamic properties with calculations and other available experimental results, thus convincingly proving the validity of our approach. The MgO X-VDOS is in remarkable agreement with *ab initio* calculations by Schütt *et al.*[22] and Ghose *et al.*[23] using DFPT within LDA and independently determined macroscopic properties (C_V, θ_D, v_D). Significant differences occur for other *ab initio* calculations.[24,25] Our experimental results therefore provide a discriminating test for the validity of the approximations made in the respective calculations. Our semi-quantitative analysis shows that the technique can be applied to a very wide class of materials and furthermore opens the possibility to study systems in extreme conditions such as high pressure and/or high temperature. This is of particular interest for geophysical studies, where, besides a host of thermodynamic properties, the determination of the VDOS in combination with low Q measurements (within the first Brillouin zone) allows the determination of v_D and v_L (average longitudinal velocity), respectively. From this, the average shear velocity v_S can be directly derived without precise knowledge of the equation-of-state.

It is worth noting that with respect to INS, the amount of material needed is three to five orders less, and anomalous absorption (like for B, Cd, Gd…) or anomalously high cross-sections (H) are not present. For multi-component systems it has to be taken into account that the X-VDOS is only defined for a particular spherical shell in Q space due to the Q dependence of the atomic scattering factor $f(Q)$. Since the scattering strengths for neutrons and x rays are essentially different, it opens the possibility to extract directly the partial densities of states in at least binary systems from coupled N-VDOS and X-VDOS measurements.

ACKNOWLEDGMENTS

The authors are grateful for many fruitful discussions with A. Chumakov, V. Kohn, and F. Sette.

[1] W. Jones and N. H. March, *Theoretical Solid State Physics* (John Wiley & Sons Ltd., London, 1973).
[2] G. Nelin and G. Nilsson, Phys. Rev. B **5**, 3151 (1972).
[3] L. M. Needham, M. Cutroni, A. J. Dianoux, and H. M. Rosenberg, J. Phys.: Condens. Matter **5**, 637 (1993).
[4] F. W. de Wette and A. Rahman, Phys. Rev. **176**, 784 (1968).
[5] G. L. Squires, *Introduction to the Theory of Thermal Neutron Scattering* (Cambridge University Press, Cambridge, 1978).
[6] M. Seto, Y. Yoda, S. Kikuta, X. W. Zhang, and M. Ando, Phys. Rev. Lett. **74**, 3828 (1995).
[7] W. Sturhahn, T. S. Toellner, E. E. Alp, X. Zhang, M. Ando, Y. Yoda, S. Kikuta, M. Seto, C. W. Kimball, and B. Dabrowski, Phys. Rev. Lett. **74**, 3832 (1995).
[8] E. Burkel, Rep. Prog. Phys. **63**, 171 (2000).
[9] D. T. Cromer and J. B. Mann, Acta Crystallogr., Sect. A: Cryst. Phys., Diffr., Theor. Gen. Crystallogr. **24**, 321 (1968).
[10] K. S. Singwi and A. Sjölander, Phys. Rev. **120**, 1093 (1960).
[11] V. G. Kohn and A. I. Chumakov, Hyperfine Interact. **125**, 205 (2000).
[12] H. J. Lipkin, Ann. Phys. (N.Y.) **18**, 182 (1962).
[13] P. Pavone, K. Karch, O. Schütt, W. Windl, D. Strauch, P. Giannozzi, and S. Baroni, Phys. Rev. B **48**, 3156 (1993).
[14] W. Windl, P. Pavone, K. Karch, O. Schütt, D. Strauch, P. Giannozzi, and S. Baroni, Phys. Rev. B **48**, 3164 (1993).
[15] J. Kulda, H. Kainzmaier, D. Strauch, B. Dorner, M. Lorenzen, and M. Krisch, Phys. Rev. B **66**, 241202(R) (2002).
[16] W. Cochran, *The Dynamics of Atoms in Crystals* (Edward Arnold, London, 1973).
[17] W. DeSorbo, J. Chem. Phys. **21**, 876 (1953).
[18] A. C. Victor, J. Chem. Phys. **36**, 1903 (1962).
[19] E. S. Zouboulis, M. Grimsditch, A. K. Ramdas, and S. Rodriguez, Phys. Rev. B **57**, 2889 (1998).
[20] H. J. Lipkin, Phys. Rev. B **52**, 10073 (1995).
[21] Y. S. Touloukian and E. H. Buyco, *Specific Heat: Non-metallic Solids* (IFI/Plenum, New York, 1970).
[22] O. Schütt, P. Pavone, W. Windl, K. Karch, and D. Strauch, Phys. Rev. B **50**, 3746 (1994).
[23] S. Ghose, M. Krisch, A. R. Oganov, A. Beraud, A. Bossak, R. Gulve, R. Seelaboyina, H. Yang, and S. K. Saxena, Phys. Rev. Lett. (to be published).
[24] N. D. Drummond and G. J. Ackland, Phys. Rev. B **65**, 184104-1 (2002).
[25] K. Parlinski, J. Łażewski, and Y. Kawazoe, J. Phys. Chem. Solids **61**, 87 (2000).
[26] G. Peckham, Proc. Phys. Soc. London **90**, 657 (1967).
[27] M. J. L. Sangster, G. Peckham, and D. H. Saunderson, J. Phys. C **3**, 1026 (1970).
[28] I. Jackson, H. Niesler, in *High Pressure Research in Geophysics*, edited by S. Akimoto and M. H. Manghnani (Center for Academic Publications Japan, Tokyo, Japan, 1982), p. 93.